Quantitative analysis of the diffusion-weighted steady-state free-precession signal in vertebral bone-marrow lesions

Andreas Biffar, MSc[1], Andrea Baur-Melnyk, MD[2], Gerwin P. Schmidt, MD[2], Maximilian F. Reiser, MD[1,2], Olaf Dietrich, PhD[1]

[1] Josef Lissner Laboratory for Biomedical Imaging, Department of Clinical Radiology – Grosshadern, LMU Ludwig Maximilian University of Munich, Germany

[2] Department of Clinical Radiology – Grosshadern, LMU Ludwig Maximilian University of Munich, Germany

ELECTRONIC PREPRINT VERSION:
This is a non-final version of an article published in final form in Investigative Radiology.
Invest Radiol 2011; **46**(10): 601–609 <URL:http://dx.doi.org/10.1097/RLI.0b013e31821e637d>.
Not for commercial sale or for any systematic external distribution by a third party.

ABSTRACT

Objectives: Diffusion-weighted steady-state free-precession (DW-SSFP) sequences have shown great potential for the differential diagnosis of benign osteoporotic and malignant neoplastic vertebral compression fractures, which appear hypo- to isointense or hyperintense in DW-SSFP MRI, respectively. In contrast to other diffusion-weighting sequences, the DW-SSFP signal depends not only on the apparent diffusion coefficient (ADC), but also on the tissue relaxation times and sequence parameters. The purpose of the present study was to provide a detailed analysis of the DW-SSFP signal in benign and malignant vertebral lesions (VLs) and in vertebral bone marrow (VBM) to understand the observed signal alterations and their dependence on tissue and sequence parameters.

Materials and Methods: MRI was performed in 40 patients with benign (n=20) or malignant (n=20) VLs to determine the fat fraction and tissue parameters (ADC, T1, T2, T2*) for both the water and fat signal. With these values, the DW-SSFP signal was simulated and compared with the measured signals for different diffusion gradients by determining the signal-intensity ratio between the SSFP signals of the lesions and of normal-appearing VBM for both malignant and benign vertebral lesions.

Results: The simulated DW-SSFP contrast agreed well with the measured contrast and provided a very good differentiation between benign osteoporotic and malignant VLs. ADCs were significantly different in both lesion types (malignant 1.36 vs. osteoporotic 1.77×10^{-3} mm²/s); however, the observed contrast differences were caused predominantly by an opposed-phase readout in combination with significantly different T2*-values (malignant 22 vs. osteoporotic 14 ms) and fat fractions (malignant 3.9 vs. osteoporotic 12 %) in the lesions as well as significantly different fat fractions in normal-appearing VBM (malignant 42 vs. osteoporotic 52 %) of both patient groups.

Conclusions: Although the ADCs of the evaluated malignant and benign VLs showed highly significant differences, the influence of diffusion on the DW-SSFP signal contrast is relatively low compared to other tissue parameters due to the very complex signal mechanism of the SSFP sequence. Thus, the observed DW-SSFP signal contrast of different vertebral lesions (hypo-/isointense vs. hyperintense signal) is rather fat- and T2*-weighted than diffusion-weighted. The intermediate diffusion weighting of the applied SSFP sequence, however, helps to shift the different contrasts into a signal range that is easily visually accessible.

Keywords:
Diffusion-weighted magnetic resonance imaging; Steady-state free precession; Spine; Bone marrow; Vertebral compression fractures

Corresponding Author:
Olaf Dietrich, PhD
LMU Ludwig Maximilian University of Munich
Josef Lissner Laboratory for Biomedical Imaging
Department of Clinical Radiology – Grosshadern
Marchioninistr. 15
81377 Munich, GERMANY
Phone: +49 89 7095-4622, Fax +49 89 7095-4627
E-mail: od@dtrx.de

Introduction

Diffusion-weighted MR imaging (DWI) has shown to be a very promising technique with clinical applications in various organs (and in particular in the brain) [1-6]. In order to perform DWI, several MRI pulse sequence types can be diffusion-sensitized by inserting additional gradient pulses [7]. Typically, a pair of gradients is used as originally suggested by Stejskal and Tanner [8]; in this case, the sequence has a well defined diffusion weighting (b-value) depending (only) on the properties of these gradient pulses.

However, a somewhat more complicated approach can be used for DWI with certain steady-state free-precession (SSFP) sequences; namely, with the contrast-enhanced Fourier-acquired steady-state technique (CE-FAST) or (synonymously) the reverse fast imaging with steady-state free precession (PSIF) sequence [9, 10]. In this case, only a single (and, thus, unbalanced) diffusion gradient pulse is inserted into each sequence repetition time [11, 12]. Spins dephased by this gradient are rephased by another diffusion gradient later in the sequence scheme, however, not necessarily by the immediately subsequent one. Hence, the duration of the diffusion-sensitizing preparation can be very different for the spins that contribute to the observed signal and the diffusion weighting cannot easily be determined, but depends in a complicated way on the relaxation times of the tissue, T_1, T_2, and on the sequence parameters, T_E, T_R, and the flip angle [13-17].

Although diffusion quantification is very difficult with the diffusion-weighted SSFP (DW-SSFP) sequence, this sequence has shown to be extremely valuable for the differential diagnosis of different types of vertebral compression fractures based on a qualitative (visual) evaluation. As demonstrated first by Baur et al., benign osteoporotic fractures appear hypointense or isointense in DW-SSFP images, while malignant lesions caused by bone-marrow tumors and metastases appear hyperintense [18]. This differentiation is highly relevant in MRI of the spine since an accurate diagnosis is important for appropriate treatment and prognosis. This is particularly significant, since both lesion types are characterized by an easily confusable appearance on conventional MR images, i. e., a hypointense signal on T_1-weighted images and a hyperintense signal on T_2-weighted or STIR images [19-21]. Several similar studies of vertebral compression fractures using qualitative DWI were performed [22-31], most of them being compatible with a general tendency to hypointensity in benign and to hyperintensity in malignant lesions. A recently published statistical meta-analysis by Karchevsky et al. [32] concluded that a hypointense signal in a fractured vertebra on DWI is strongly suggestive of a benign etiology.

However, a theoretical analysis of the measured DW-SSFP signal in vertebral bone marrow (VBM) has not been performed yet and a physical understanding of the observed signal contrast is still lacking. The purpose of the present study was, therefore, to provide a detailed analysis of the DW-SSFP signal in VBM and in benign as well as in malignant vertebral lesions (VLs) in order to understand the observed signal alterations and their dependence on tissue and sequence parameters.

Materials and Methods

In order to analyze the signal dependencies of the DW-SSFP sequence in vertebral lesions, we established a theoretical description of the DW-SSFP signal in the spine and then performed a patient study, in which we determined all required independent parameters for normal-appearing VBM, for the intervertebral discs (IVDs), and for different vertebral lesion types.

Theory

The formation of the NMR SSFP signal in the presence of an additional constant diffusion-sensitizing gradient was first studied by Kaiser et al. [13]. This analysis was extended to the case of pulsed field gradients by Wu et al. [14]. They derived the signal infinitesimally short after (S^+, FID component) and before (S^-, SSFP echo component) the application of the RF pulse for a diffusion gradient pulse of duration δ and strength G. The signal of S^- corresponds to the diffusion-weighted signal measured with a CE-FAST or PSIF sequence [11, 12]. The average transverse magnetization of the DW-SSFP sequence is then given by [15, 17]

$$S_\perp^- = -\frac{M_0(1-E_1)E_2A_2^{1/3}\left(F_1 - E_2A_1A_2^{-2/3}\right)\sin(\alpha)}{r - s\,F_1} \quad \text{Eq. [1]}$$

with

$$F_1 = K - \sqrt{K^2 - A_2^{-2}}$$

$$K = \frac{1 - E_1A_1\cos(\alpha) - E_2^2A_1^2A_2^{2/3}(E_1A_1 - \cos(\alpha))}{E_2A_1A_2^{4/3}(\cos(\alpha)+1)(1-E_1A_1)}$$
$$r = 1 - E_1\cos(\alpha) + E_2^2A_1A_2^{-1/3}(\cos(\alpha) - E_1)$$
$$s = E_2A_1A_2^{4/3}(1 - E_1\cos(\alpha)) + E_2A_2^{1/3}(\cos(\alpha) - E_1)$$
$$A_1 = \exp(-(\gamma G\delta)^2 T_R \cdot D), \qquad A_2 = \exp(-(\gamma G\delta)^2\delta \cdot D)$$
$$E_1 = \exp(-T_R/T_1), \qquad E_2 = \exp(-T_R/T_2).$$

Required input parameters are the tissue properties such as the (apparent) diffusion coefficient (ADC), D, and the relaxation times, T_1, T_2, as well as the sequence timing parameters, T_R, T_E, and the flip angle, α. This model is based on the hypothetical assumption that the signal is measured infinitesimally short before the application of the RF pulse. In the case of the assessed PSIF sequence, the signal is acquired as a gradient-shifted echo [9] and its dependence on the echo time, T_E, of the DW-SSFP sequence, i. e., the time span between the acquisition of the k-space center and the center of the subsequent RF pulse, has to be considered. First, an additional attenuation of the signal caused by the T_2*-decay [9, 10] leads to

$$S_\perp(T_E) = S_\perp^- \cdot \exp(-T_E/T_2^*)$$

While in most parts of the body the T_2*-decay is negligible for typical PSIF echo times of 5 to 10 ms, T_2* is strongly reduced in vertebral bodies due to the difference in magnetic susceptibility between trabecular bone and bone marrow [33, 34], and the T_2*-weighting has to be considered for the signal analysis in the spine.

Furthermore, the signal in VBM is a combined function of the signal components of fat and water. Since protons in both components are characterized by different physical properties, the exact distribution pattern in terms of the fat, f_{fat}, and water fraction , $f_{water} = 1 - f_{fat}$, has to be known. In addition, the relative phase between the signals of the fat and water component, depending on T_E, plays an important role for the signal characteristics. Hence, the combined signal is given by

$$S_{VBM} = f_{water}S_{\perp,water}^- \exp(-T_E/T_{2,water}^*) + f_{fat}S_{\perp,fat}^- \exp(-T_E/T_{2,fat}^*)\exp(-i\Delta\omega_{fw}T_E) \qquad \text{Eq. [2]}$$

with $\Delta\omega_{fw} = 2\pi\Delta f_{fw}$, where Δf_{fw} is the difference between the precession frequencies of fat and water, the chemical shift. $S_{\perp,water}^-$ and $S_{\perp,fat}^-$ are defined as the average transverse magnetizations of both components according to Eq. [1]. Depending on the choice of T_E, two distinguished cases can be differentiated, the opposed-phase case $\exp(-i\Delta\omega_{fw}T_{E,opp}) = -1$, in which the signal corresponds to the absolute value of the signal difference of both components, and the in-phase case $\exp(-i\Delta\omega_{fw}T_{E,in}) = +1$, in which the signal corresponds to the absolute value of the sum of both components. In summary, the signal in VBM is a function of 9 independent parameters: $T_{1,water}$, $T_{1,fat}$, $T_{2,water}$, $T_{2,fat}$, $T^*_{2,water}$, $T^*_{2,fat}$, ADC_{water}, ADC_{fat}, and f_{fat}.

Patient selection

After internal review board approval and informed consent had been received, the protocol was applied to 51 patients. Inclusion criteria for this study were the suspicion of acute vertebral fracture based on either pathological findings in alternate image studies and/or patient history. A fracture was considered to be acute if the patients suffered from back pain and an edema, appearing as a hyperintense region on the STIR image, was apparent. Exclusion criteria were sheer traumatic fracture, an underlying hematologic disease or, in the case of malignant lesions, a treatment with radiation or chemotherapy or radiation therapy. 6 patients with osteoporotic fractures were excluded from the signal analysis because no acute edema was found in the fracture site. In the case of the patients with malignant lesions, 5 patients were excluded prior to the signal analysis because all vertebral bodies were diffusely infiltrated and the relative signal contrast between normal appearing vertebral bone marrow and the lesions could not be determined. The mean fracture age of the patients included in the signal analysis was 18 days. The majority of the lesions was located between T9 and L5 (35/40, 88%).

The patient collective was divided into two groups: Group 1 consisted of 20 patients with acute osteoporotic fractures (14 women and 6 men, median age: 72 years, range: 52–86 years). The presence of a tumor in these patients was ruled out by follow-up MRI or multidetector computed tomography (CT) examinations and clinical follow up over 1 year. In case of a finding of a fracture of unclear etiology or an unclear bone-marrow lesion, histological clarification was obtained ($n = 2$) and no malignancy was found. Group 2 consisted of 20 patients with malignant infiltrations (10 women and 10 men, median age: 60 years, range: 25–87 years) accompanied by pathological fractures in 13

of these 20 cases. Primary neoplasms included breast cancer ($n = 6$), plasmacytoma ($n = 4$), adenocarcinoma ($n = 3$), ovarian cancer ($n = 1$), hypopharyngeal cancer ($n = 1$), thyroid carcinoma ($n = 1$), bladder cancer ($n = 1$), pancreatic cancer ($n = 1$), lung cancer ($n = 1$) and non-seminoma ($n = 1$). The diagnoses were confirmed by histopathological examination ($n = 18$) of specimens obtained during surgery, CT-guided biopsy, or follow-up MRI examinations (exclusion of a benign cause of the VL based on growth dynamic of the lesion, diffuse infiltration of other vertebrae, the involvement of posterior elements, or paravertebral tumorous soft tissue) ($n = 2$).

MRI procedure

Morphological imaging

Measurements were performed on a 1.5-T whole-body scanner (MAGNETOM Avanto, Siemens Healthcare, Erlangen, Germany). Prior to the quantitative and DW-SSFP measurements, T_1-weighted (T_R/T_E, 531/12 ms), STIR ($T_R/T_E/T_I$, 3790/61/180 ms) and T_2-weighted (T_R/T_E, 4420/118 ms) turbo-spin-echo images of 21 sagittal slices with a slice thickness of 3 mm were acquired using a 44×44 cm² field of view (FOV) and a matrix size of 384×384. These pre-contrast images were used for lesion localization and proper slice positioning of the following quantitative measurements.

Vertebrae of each patient were classified into the categories normal-appearing VBM or VL according to their appearance on the T_1-weighted, T_2-weighted and STIR images by the consensus decision of two experienced radiologists. If present, any additional old fractures (without any signs of bone-marrow edema on the STIR image) or diffusely infiltrated vertebrae (manifested as a homogeneous signal reduction on unenhanced T_1-weighted images) were excluded from the analysis. For the analysis of the signal in the IVDs, those showing signs of degeneration either in form of a dehydration of the nucleus pulposus (indicated by a signal loss on T_2-weighted images) or by clefts in the annulus fibrosus (showing an increased signal on contrast-enhanced T_1-weighted images) were excluded.

Parameter quantification

T_1-, T_2- and ADC-values were quantified using the techniques presented recently by Biffar et al. [35]. In short, single-shot turbo-spin-echo (ssTSE) sequences in sagittal orientation with either fat-suppression or water-suppression pulses were used for all quantitative measurements; for T_1-quantification, the ssTSE measurement was performed as saturation-recovery experiment with 8 different saturation times between 5 and 3200 ms; for T_2-quantification, the ssTSE measurement was performed with 6 different echo times between 14 and 170 ms. ADCs were determined with a diffusion-weighting ssTSE sequence with 4 different b-values between 100 and 600 s/mm². Parameters were then quantified on a region-of-interest (ROI) basis, in one VL, one IVD, and one normal-appearing vertebra per patient. In case of the fracture, the ROI appearing hyperintense on the STIR-image was selected. In case of normal appearing vertebral bodies and the intervertebral discs, the whole body or disc was selected.

For the determination of $T^*_{2,water}$ and $T^*_{2,fat}$, a multi-echo spoiled gradient-echo sequence was used, preceded either by a fat- or a water-saturation pulse, respectively. Echoes were acquired at $T_E = 5$, 10, 15, and 20 ms. The sequence parameters were set to $T_R = 197$ ms, FOV 300×225 mm², slice thickness 5 mm, receiver bandwidth 260 Hz/pixel, flip angle 25° and a matrix size of 128×96. The T_2^*-values were calculated, using the ROIs applied for the quantification of the other parameters. The signal intensities were fitted to a monoexponential decay model as a function of the varying T_E.

For the quantification of f_{fat}, opposed- and in-phase images were acquired with a spoiled gradient-echo sequence ($T_{E,opp} = 2.38$ ms, $T_{E,in} = 4.76$ ms, FOV 300×225 mm², slice thickness 5 mm, matrix size 320×240). f_{fat} was determined using the ROIs applied for the quantification of the other parameters. An extended two-point Dixon method, using the uwrapped phase information of the opposed-phase image, was applied [36-38].

DW-SSFP measurements

For the experimental analysis of the signal behavior of the DW-SSFP sequence, we acquired a sagittal slice (corresponding to the slice selected for the quantitative measurements described in the previous section) with 5 different diffusion-gradient durations. The diffusion gradient was applied in read-out direction and its amplitude was kept constant at 23 mT/m, while the duration of the diffu-

sion gradient was varied (δ = 0.5, 1.5, 3.0, 5.0, 7.4 ms). Following the original approach by Baur et al. [18], the other sequence parameters were set to: a 256×192 matrix, T_E = 7.17 ms, corresponding to the opposed-phase situation, T_R = 25 ms, flip angle 40°, slice thickness 5 mm, a receiver bandwidth of 100 Hz/pixel, and a FOV of 300×225 mm². Signal intensities were evaluated in ROIs corresponding to those used in the parameter quantification described above. In addition, the influence of noise was determined based on the ratio, ψ, of foreground signal and background noise intensities at the shortest diffusion gradient duration, δ, for the IVD ROI used above; the noise was measured as the mean signal, S_{Noise}, in a background ROI placed behind the spine in each patient and ψ was defined as $\psi = S_{IVD}(0.5ms) / S_{Noise}$.

DW-SSFP simulations

We determined the mean values of all parameters for normal-appearing VBM, IVDs, and VLs separately in both patient groups. Based on these values, the signal was simulated in normal-appearing VBM, IVDs, and both types of VLs for the in- and opposed-phase scenario, using Eq. [2]. At higher diffusion weightings, the signal is dominated by noise. Therefore, the simulated signal, S_{sim}, was superimposed by a noise signal corresponding to the measured value of ψ and is given by

$$S_{\mathrm{sim}} = \sqrt{\left|S_{\mathrm{VBM,sim}}\right|^2 + \left|S_{\mathrm{IVD,sim}}(0.5\ \mathrm{ms})/\psi\right|^2}$$

Based on these simulations, the signal ratio between both types of VLs and normal-appearing VBM, $R_{VL} = S_{VL}/S_{VBM}$, was calculated. This ratio is a quantitative measure corresponding to the qualitative assessment of tissue contrast in terms of hyper- ($R_{VL} > 1$), iso- ($R_{VL} \approx 1$) and hypo-intensity ($R_{VL} < 1$).

The individual influence of the different tissue parameters ($T_{1,water}$, $T_{1,fat}$, $T_{2,water}$, $T_{2,fat}$, $T^*_{2,water}$, $T^*_{2,fat}$, ADC_{water}, ADC_{fat}, and f_{fat} of both the normal-appearing VBM and the lesion) on the observed visible contrast was assessed by simulating the signal ratio, R_{VL}, for diffusion gradients with durations $0 \le \delta \le 9$ ms. For these simulations, all parameters except the one under consideration were set to their mean values over both patient groups; thus, the influence of a single parameter could be analyzed. We calculated the mean values of R_{VL} over all diffusion weightings separately for both patient groups as well as the mean value of the contrast difference, i. e.,

$\mathrm{mean}_\delta\ [R_{VL}(\delta, \text{malignant}) - R_{VL}(\delta, \text{osteoporotic})]$.

Statistical analysis

For each measured parameter, the mean values and standard deviations in normal-appearing VBM, IVDs and both types of VLs were determined for each patient group separately. An unpaired two-tailed t-test was performed to compare each parameter between both patient groups. A paired t-test was performed to compare each parameter between normal-appearing VBM, IVDs, and VLs within each patient group. The p-value indicating significant difference was chosen to be < 0.05.

We determined the specificities, sensitivities, and accuracies for the diagnosis of a malignant infiltration based on the signal ratio, R_{VL}, of the DW-SSFP measurements at different diffusion weightings. This diagnosis was made with a cut-off value $R_{VL,cut\text{-}off}$; i. e., a malignant lesion was diagnosed for a signal ratio $R_{VL} \ge R_{VL,cut\text{-}off}$, and a benign lesion otherwise. This diagnosis was then compared with the reference diagnosis. As a cut-off value, the parameter yielding the highest accuracy (i. e., the highest proportion of true results in the population) was chosen. An additional analysis was performed with a fixed cut-off value of $R_{VL,cut\text{-}off} = 1.2$, approximately corresponding to the qualitative evaluation in former studies that differentiated between hyperintense ($R_{VL} \ge 1.2$) vs. hypo- or isointense ($R_{VL} < 1.2$) signal.

Statistical analysis was performed by using R for Linux, release 2.10.0 (R: A Language and Environment for Statistical Computing, R Foundation for Statistical Computing, Vienna, Austria, <http://www.R-project.org> [39]).

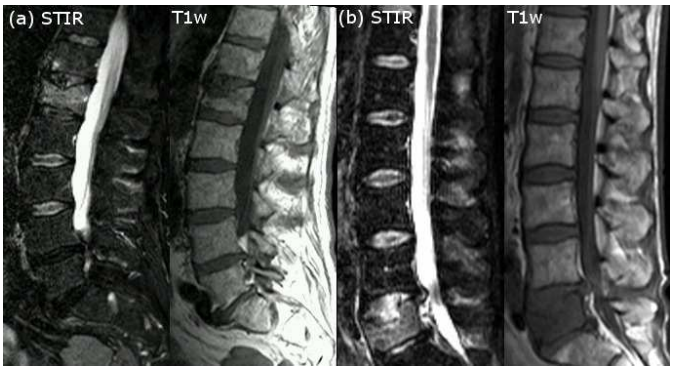

Figure 1: T_1-weighted and STIR images of (a) a patient with an osteoporotic VL in L1 and (b) a patient with a malignant VL in L5.

Results

Exemplary images of the morphological sequences that were used for diagnosis, slice positioning of the quantitative and DW-SSFP images and for lesion localization are shown in Fig. 1.

Parameter quantification

Results of previous studies suggest that the ADC of protons in fat is very close to 0 [40, 41] (Lehnert et al. determined ADCs for fat molecules in vivo ranging from 0.01 to 0.02×10^{-3} mm^2/s, which is about a factor of 50 lower than the ADCs of water molecules in VBM) and, therefore, ADC_{fat} was set to 0 throughout the study and only determined in water. In the VLs and IVDs, the values of the relaxation times T_1, T_2, and T_2^* of the fat component could not be determined due to the very low fat content in the lesions (and in the IVDs) and the slight imperfections of the water suppression; as a consequence, the measured signal in these tissues is a mixture of the very small fat signal and the remaining (imperfectly suppressed) water signal. In the IVDs, the water fraction was not determined but set to 100 %. The mean values and standard deviations of the other parameters are summarized in Table 1. Comparing normal-appearing VBM and VLs within each patient group, significant differences ($p < 0.001$) were found for all parameters. The comparison of both patient groups showed that $T_{1,fat}$, $T_{2,fat}$, and f_{fat} of normal-appearing VBM as well as ADC_{water}, $T^*_{2,water}$ and f_{fat} of the VLs differed significantly. In the case of the IVDs, significant differences between both groups were only found for $T_{1,water}$.

Signal measurements

Images acquired with the DW-SSFP sequence in two exemplary patients at different diffusion-gradient durations are shown in Fig. 2. The osteoporotic VL appears hypointense compared to the adjacent normal-appearing vertebrae, while the pathological VL appears hyperintense. The mean values of R_{VL} for each δ for both patient groups are summarized in Table 2. At each δ, we compared the R_{VL}-values between both patient groups and a significant difference ($p < 0.001$) was found for each δ. We calculated the sensitivities, specificities, and accuracies with regard to the diagnosis of a malignant lesion based on the R_{VL}. The results are summarized in Table 3. The highest sensitivity (95%) and specificity (100%) was found for a δ of 1.5 ms and a cut-off of $R_{VL,cut\text{-}off} = 1.82$. If we fix the cut-off to $R_{VL,cut\text{-}off} = 1.2$, the highest accuracy was found for $\delta = 5.0$ ms. The ratio of the IVD signal and the background noise intensity were found to be almost equal in both patient groups at $\psi \approx 10.8\pm2.9$.

Signal simulations

Using the determined parameters, simulations of the SSFP signal were performed for both patient groups and an opposed- and in-phase scenario. The opposed-phase signal curves in normal-appearing VBM, IVDs, and VLs as a function of the duration of the diffusion gradient, δ, are shown in Fig. 3. The signal in osteoporotic VLs is hypointense relative to normal-appearing VBM, while the signal is clearly hyperintense in malignant VLs. Comparing the simulated absolute values of the signal in both types of VLs, a strongly increased signal by a factor of ≈ 2 is found in pathological VLs. Conversely, the signal of normal-appearing VBM is strongly increased in the osteoporotic group by a factor of ≈ 2. In the IVDs, the signals are comparable in both patient groups.

The ratios R_{VL} for the in- and opposed-phase situation are shown in Fig. 4. For the opposed-phase scenario, R_{VL} is strongly increased (indicating hyperintensity of the lesion) in the group with malignant infiltrations compared to the osteoporotic group. For the in-phase scenario, the differences between both situations are strongly reduced. The comparison of the measured and the simulated signal ratios, R_{VL}, is shown in Fig. 5. A good agreement between both was found, except for the highest value of $\delta = 7.4$ ms.

Finally, the analysis of the influence of the individual tissue parameters on the observed contrast is shown in Fig. 6. The greatest contributions to the observed total contrast result from the differences (between both patient groups) of f_{fat} in the lesions as well as in normal-appearing VBM, of $T^*_{2,fat}$ in normal-appearing VBM, and of $T^*_{2,water}$ in the lesions. Smaller effects are caused by the differences of $T_{1,fat}$ and $T_{2,fat}$ in normal-appearing VBM and (with opposite sign) of $T_{2,water}$ in the lesions. The other parameter differences do not contribute substantially to the observed contrast.

Table 1: Mean values (standard deviations) of the parameters determined in normal-appearing vertebral bone marrow (VBM), intervertebral discs (IVDs), and vertebral lesions (VLs) of both patient groups

	Osteoporotic lesion ($n = 20$)			Malignant lesion ($n = 20$)		
	VBM	IVD	VL	VBM	IVD	VL
$T_{1,water}$ [ms]	925 (101)	955 (140)	1331 (170)	927 (108)	1112 (215)	1264 (150)
$T_{1,fat}$ [ms]	279 (30)*	–	–	375 (118)*	–	–
$T_{2,water}$ [ms]	82 (15)	65 (14)	120 (27)	86 (16)	78 (26)	108 (25)
$T_{2,fat}$ [ms]	172 (14) †	–	–	149 (20) †	–	–
$T^*_{2,water}$ [ms]	8 (3)	42 (20)	14 (6) ‡	8 (4)	36 (16)	22 (10) ‡
$T^*_{2,fat}$ [ms]	11 (3)	–	–	9 (3)	–	–
ADC_{water} [10^{-3} mm^2/s]	0.58 (0.14)	1.76 (0.36)	1.77 (0.26) ¶	0.58 (0.18)	1.87 (0.29)	1.36 (0.39) ¶
f_{fat} [%]	52 (13) §	–	12 (12) #	42 (16) §	–	3.9 (3.8) #

*, †, ‡, ¶, §, #: Significant differences between osteoporotic and malignant group; the corresponding p-values are: * $p = 0.002$, † $p < 0.001$, ‡ $p = 0.001$, ¶ $p < 0.001$, § $p = 0.048$, and # $p = 0.011$.

Table 2: Mean values (standard deviations) of the signal ratio, $R_{VL,}$ between the vertebral lesion (VL) and normal appearing vertebral bone marrow for patients with osteoporotic and malignant VLs at different durations, δ, of the diffusion weighting gradient

R_{VL}	Osteoporotic lesion	Malignant lesion	p-value
δ = 0.5 ms	1.01 (0.38)	3.43 (1.93)*	< 0.0001
δ = 1.5 ms	0.97 (0.38)	3.40 (1.81)*	< 0.0001
δ = 3.0 ms	0.85 (0.31)	2.80 (1.42)*	< 0.0001
δ = 5.0 ms	0.69 (0.20)	2.06 (0.84)*	< 0.0001
δ = 7.4 ms	0.69 (0.19)	1.23 (0.42)*	< 0.0001

* significant difference ($p < 0.05$) between osteoporotic and malignant group

Table 3: Sensitivities, specificities, and accuracies for diagnosing a malignant lesion based on R_{VL}

	optimized R_{VL} cut-off				fixed cut-off ($R_{VL,cut\text{-}off} = 1.2$)		
δ [ms]	cut-off	sensitivity	specificity	accuracy	sensitivity	specificity	accuracy
0.5	1.85	85	100	93	100	70	85
1.5	1.82	95	100	98	100	75	88
3.0	1.52	90	100	95	95	80	88
5.0	1.29	85	100	93	85	95	90
7.4	0.98	79	95	87	53	95	74

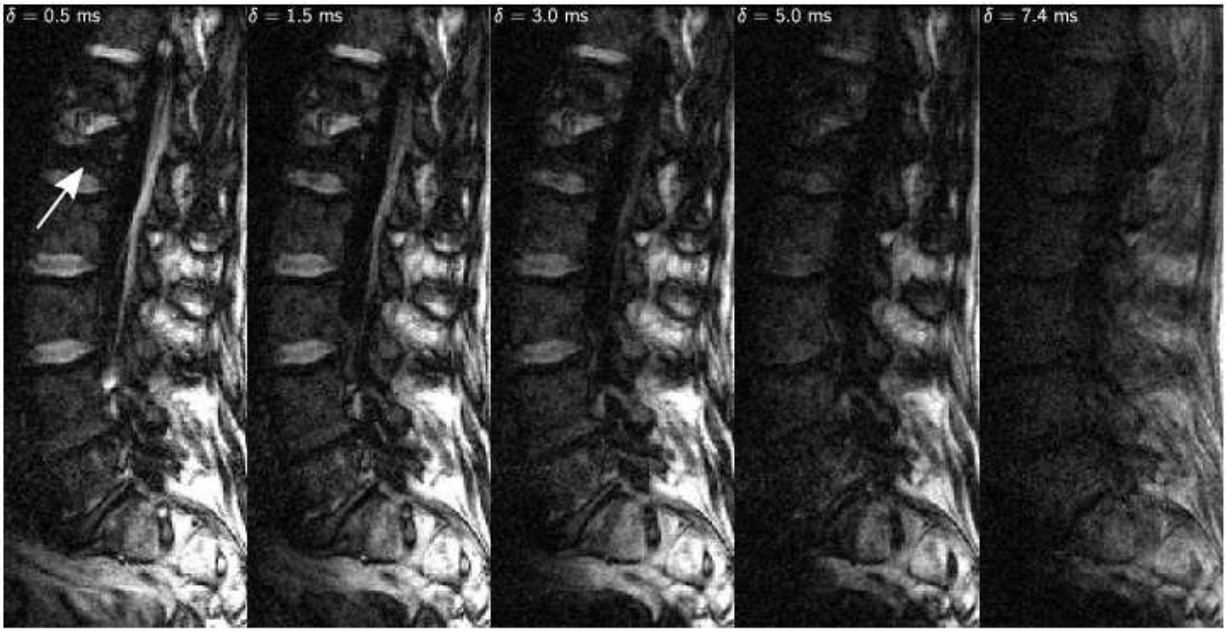

(a) Osteoporotic lesion

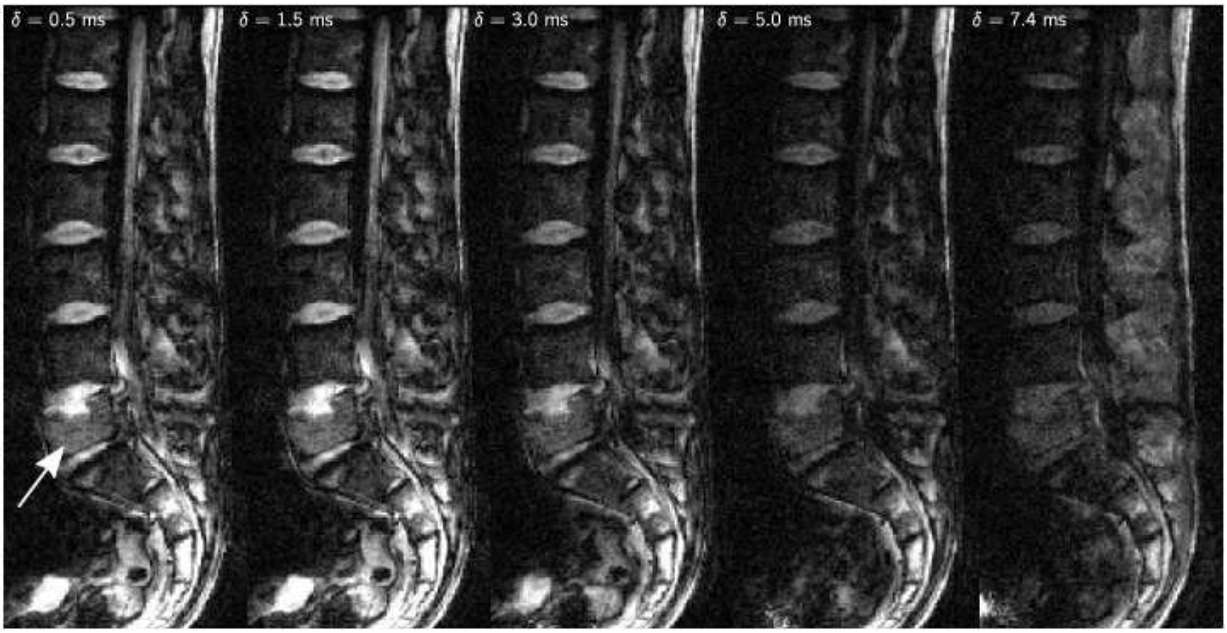

(b) Malignant lesion

Figure 2: DW-SSFP images of (a) a patient with an osteoporotic VL in L1 and (b) a patient with a malignant VL in L5 (arrows point at the VLs). Images were acquired with a constant amplitude and a variable duration, δ, of the diffusion gradient.

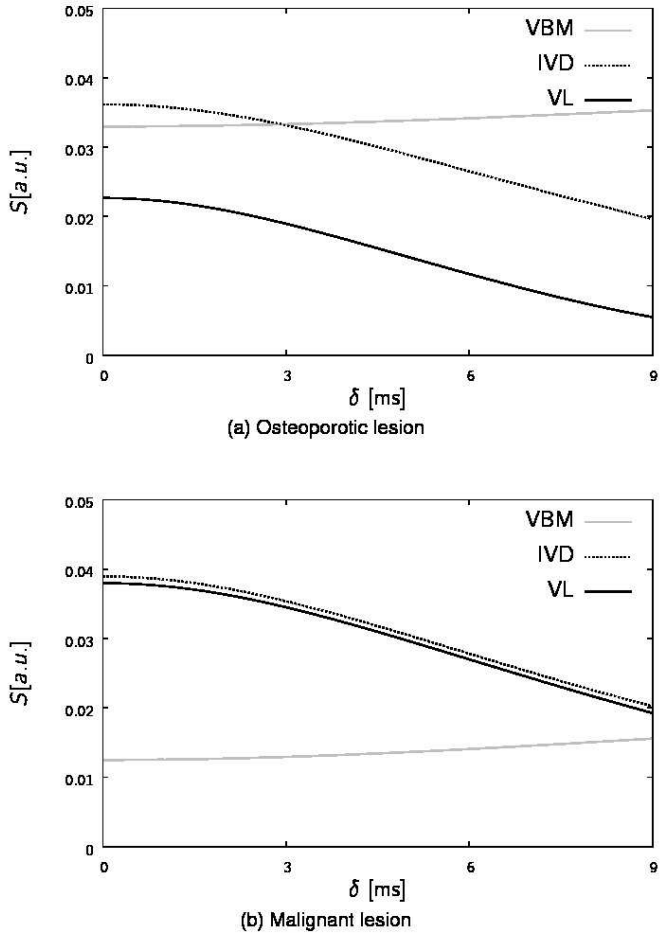

Figure 3: Simulation of the DW-PSIF signal in normal-appearing VBM (gray line), IVDs (dashed line) and VLs (black line) of (a) patients with an osteoporotic VL and (b) patients with malignant lesions at an opposed-phase T_E of 7.17 ms.

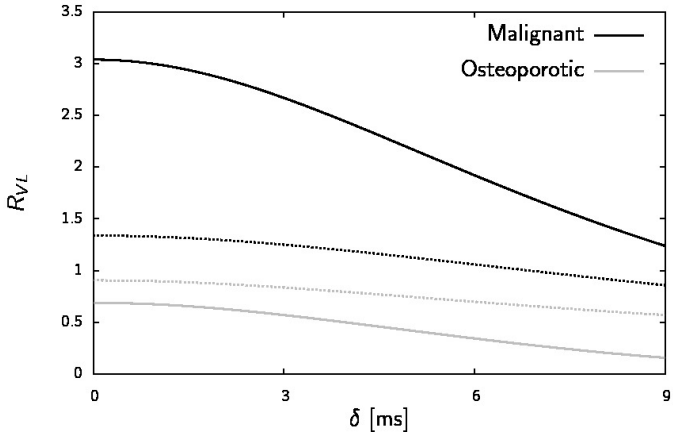

Figure 4: Simulation of the signal ratio, R_{VL}, between the DW-PSIF signal of a VL and of normal-appearing VBM as a function of the diffusion gradient duration, δ. Shown are the results for the opposed-phase ($T_E = 7.17$ ms, solid line) and in-phase situation ($T_E = 9.53$ ms, dashed line).

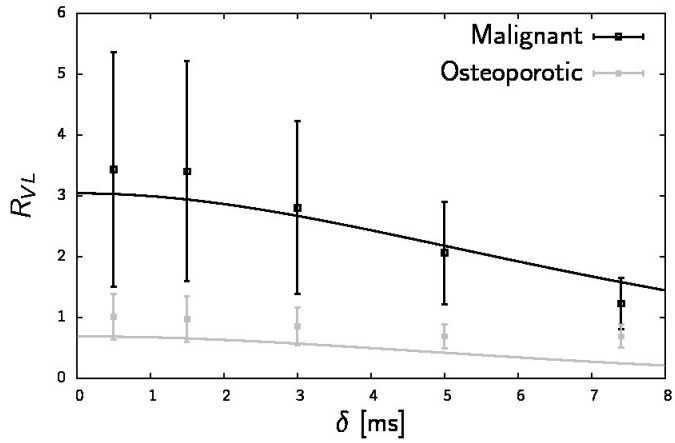

Figure 5: Comparison between the measured mean values of R_{VL} (squares with errorbars) and the simulated values (solid lines) based on the parameters. The length of the errorbars corresponds to the twice the standard deviation.

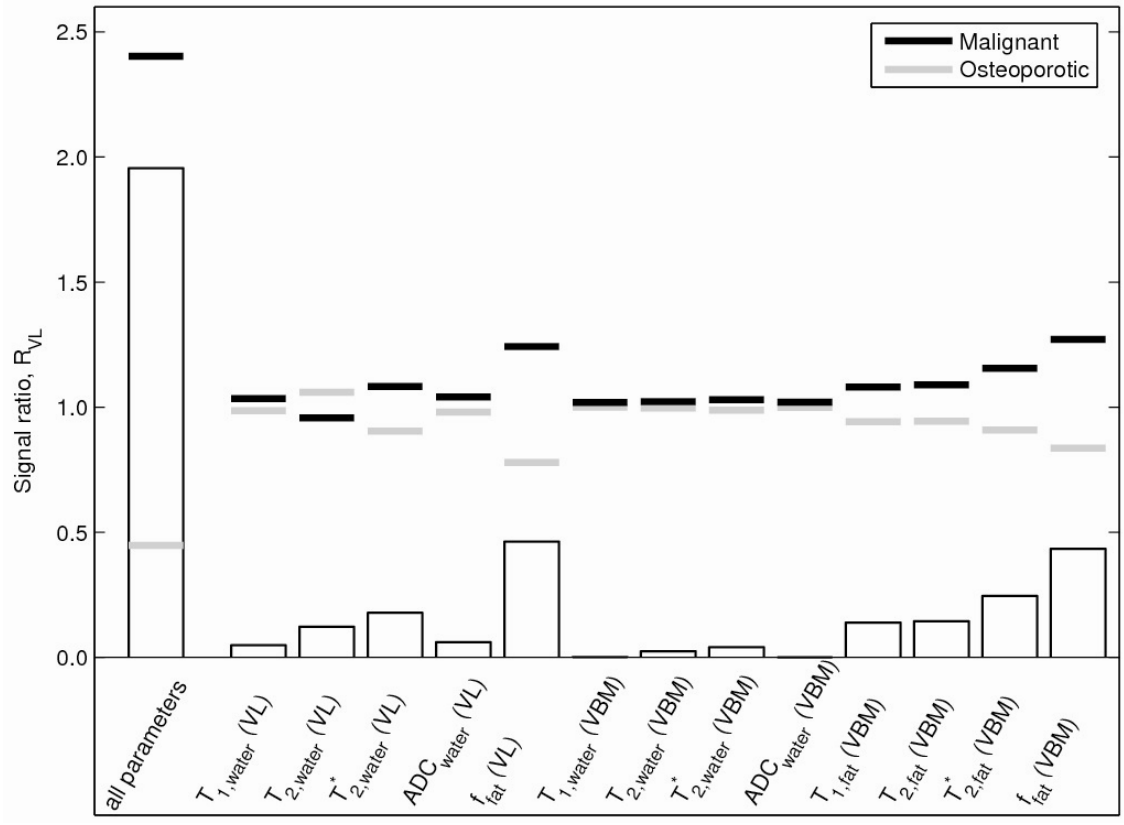

Figure 6: Influence of the different tissue parameters on the simulated signal ratio, R_{VL}. All parameters except the one given at the horizontal axis were set to the mean value of both patient groups. The solid horizontal lines indicate the mean values of the signal ratios, R_{VL}, averaged over all evaluated diffusion weightings (gradient duration $0 \le \delta \le 9$ms) for malignant or osteoporotic lesions. The bars correspond to the average contrast difference between both patient groups.

Discussion

In the past, the DW-SSFP sequence has been applied successfully for the differential diagnosis of benign and malignant lesions in the spine in various studies [32, 42]. However, the setting of important sequence parameters either differed or is not reported in the literature. Furthermore, the general hypothesis that the observed contrast originates from the different diffusion characteristics of both lesion types has never been validated. In the following, we discuss both issues based on our signal simulations and measurements of the DW-SSFP sequence.

Signal model

The PSIF echo signal of the evaluated DW-SSFP sequence is a complicated function of several tissue and sequence parameters as summarized in Eqs. [1] and [2]. Thus, measurement errors in all quantified parameters might result in deviations between the simulated signals and the actually – and independently – measured signals of the DW-SSFP sequence. However, as shown in Fig. 4, the measured signal ratios agree well with our signal simulations (which did not contain any free parameters), indicating that our theoretical signal model is valid for the present application – in particular, we need not consider the slightly more complex model suggested by Freed et al. [16]. The observed deviations at the highest diffusion weightings might be related to some approximations we had to use in our signal model: we could not determine the relaxation parameters of the (relatively small) fat component in the VLs with sufficient accuracy. Thus, we had to use $T_{1,fat}$ and $T_{2,fat}$ determined in normal-appearing VBM as well as $T^*_{2,water}$ determined in the VLs for our simulations of the VL fat signal. The contribution of this fat signal to the total signal increases at longer diffusion gradients due to the diffusion attenuation of the water signal, and might explain the observed deviations.

Lesion differentiation

The presented patient measurements with the DW-SSFP sequence yielded an excellent differentiation

of both fracture types based on R_{VL} with a specificity of 95 % and a sensitivity of 100 % for $\delta = 1.5$ ms. In previous studies, the classification was performed using a qualitative criterion (the subjectively evaluated relative signal contrast) and, therefore, the results cannot be compared directly. Still, the cut-off value of 1.52, found at $\delta = 3.0$ ms, agrees approximately with the qualitative result that hypo- and isointensity of the VLs are an indicator for a benign cause [27]. If we fix the cut-off to the lower value of $R_{VL,cut\text{-}off} = 1.2$ (as a better approximation to the visual evaluation), good accuracies of 88 to 90% are found for $\delta = 1.5\ldots5.0$ ms in agreement with earlier studies [23].

We chose the signal ratio $R_{VL} = S_{VL}/S_{VBM}$ of the signal intensity in the lesion relative to the neighboring normal-appearing VBM as the target quantity of our analysis. Alternatively, the signal difference $D_{VL} = S_{VL} - S_{VBM}$ or the signal-difference-to-noise ratio $D_{VL}/$ could have been used. Although the latter might be more common in MR signal analyses, we preferred the signal ratio since it is both closest to the established visual image evaluation and it enables us to define unambiguous cut-off values for the diagnosis. The absolute signal as well as the signal difference (whether normalized to the noise level or not) depend on the MRI system, the receiver coil, and, e. g., the size of the patient; thus, it is not possible to define a cut-off value as for the signal ratio.

The analysis of the relative signal contrast or of R_{VL} allows to differentiate between the fracture types, but – based on the measurements alone – it remains unclear whether the measured differences originate from the normal-appearing VBM, the VLs, or both (since only signal ratios, but not absolute signal intensities can be compared between both patient groups). To overcome this limitation, the signal of the IVDs can be used as reference signal, since we found the tissue parameters of the IVDs to be comparable between both patient groups (cf. Table 1). For example, at a diffusion gradient duration of $\delta = 5$ ms, the measured signal ratio between normal-appearing VBM and IVDs is 0.53 in patients with tumors and 0.69 in osteoporotic patients. The signal ratio between VLs and IVDs is 0.89 for malignant lesions and 0.46 for osteoporotic lesions. This demonstrates that indeed two opposite effects contribute to the observed signal ratios: the normal-appearing bone marrow exhibits higher signal in osteoporotic patients, while simultaneously the lesions have a higher signal in the patients with pathological lesions.

These observations agree again well with the simulated curves shown in Fig. 2, which also demonstrate the increased signal in normal-appearing VBM of osteoporotic patients (by a factor of ≈ 2) and the decreased signal of the osteoporotic lesions (again by a factor of ≈ 2).

In this study, we did not differentiate between different tumor types; this should be done in future studies with a larger patient collective to exclude a potential bias caused by different characteristics of the tumors.

In- and opposed-phase effects

Figure 3 demonstrates that the differential diagnosis based on the relative signal contrast in both patient groups is only feasible in the opposed-phase state. In the in-phase situation, a differentiation based on this contrast, i. e., in terms of hypo- and hyperintensity of the lesion, is hardly possible.

To understand this difference, we first consider the signal in the opposed-phase situation. For example, at a diffusion gradient duration, δ, of 3 ms, the signal intensity of the fat component of normal-appearing VBM is 2–3 times larger than the signal of the water component. Thus, the measured signal of VBM corresponds to the fat signal minus the water signal for both patient groups, while the signal of the VLs corresponds to the water signal minus the fat signal due to the lower value of f_{fat}. Hence, the increased value of f_{fat} in normal-appearing VBM of the osteoporotic group causes an increased signal compared to the malignant group, while the opposite effect occurs in case of the VLs, i. e., the increased value of f_{fat} in the osteoporotic VLs causes a decrease of the signal compared to the malignant lesions. Since the signal of the VL appears in the numerator and the signal of normal-appearing VBM in the denominator of R_{VL}, both effects together cause the strong difference between both patient groups.

In the in-phase situation, these effects cannot be observed, since in normal-appearing VBM as well as in the VLs the signal corresponds to the sum of the water and fat signal. This demonstrates the importance of the right choice of the echo time, T_E, for a differential diagnosis between both lesion types. The original studies by Baur et al. [18, 23, 27]

were based on a DW-SSFP sequence with an opposed-phase readout. Unfortunately, in other previous studies, the exact value of T_E is not given except by Byun et al. [26], who reported a T_E of 5 ms. Hence, it is not possible to check retrospectively, whether a different setting of T_E is responsible for any controversial results.

Signal weighting of the DW-SSFP sequence

As discussed above, the observed contrast between lesions and normal-appearing VBM is caused by characteristic signal changes in both tissues. In the following paragraphs, we discuss which tissue parameters are predominantly responsible for this contrast.

On the one hand, the parameters showing the largest differences between both patient groups in normal-appearing VBM were f_{fat}, $T^*_{2,fat}$, $T_{2,fat}$ and $T_{1,fat}$. Indeed, these four parameters contribute substantially to the observed contrast; particularly f_{fat} exhibits the largest influence on the contrast of all input parameters as shown in Fig. 5. Thus, the VBM signal is considerably fat-weighted. The observed increase of f_{fat} in normal-appearing VBM of patients with osteoporosis agrees well with the literature [43, 44]. It was also reported by Yeung et al. [45] that while f_{fat} increased significantly in patients with osteoporosis, no significant change of the ADC compared to healthy patients was found.

In the VLs, on the other hand, the main contributions to the contrast differences result from f_{fat} and $T^*_{2,water}$. The simulations of the signal changes show that particularly the influence of the ADC of the VLs is substantially smaller compared to the other parameters. At a δ of 3 ms, the signal decrease in the osteoporotic VLs caused by the ADC is ≈ 3 %. The contrast caused by the decreased T_2^* in the osteoporotic patient group leads to a signal decrease of ≈ 22 % compared to the malignant group. The increase of f_{fat} in the osteoporotic VLs causes a decline of the signal by ≈ 30 %. Hence, the diffusion weighting is in fact negligible compared to the other tissue properties. Combining both effects, the observed signal contrast between both patient groups at a small δ is not predominantly diffusion-weighted as it was described in the literature, but is rather fat- and T_2^*-weighted.

However, these results do not imply that the diffusion weighting of the analyzed SSFP sequence should be reduced or completely removed. Indeed, the visual (qualitative) differentiation of osteoporotic and malignant lesions depends essentially on the total signal attenuation to the point at which (practically) all osteoporotic lesions become iso- or better hypointense. As illustrated in Fig. 3 and demonstrated in Table 3, this visual differentiation works best at diffusion-gradient durations between about 3 and 6 ms, which provide high diagnostic accuracies and cut-off values not substantially greater than 1.2.

Conclusions

In the present study, we could confirm previous results that the DW-SSFP sequence provides an excellent differentiation between benign osteoporotic and malignant VLs. Based on the comparison of simulations and measurements, we were able to show that the main reason for the different contrasts are the differing fat fractions and T_2^*-values in the lesions as well as in normal-appearing VBM of both entities. Although the ADCs of the evaluated malignant and benign VLs showed highly significant differences, the influence of diffusion on the DW-SSFP signal contrast is relatively low compared to other tissue parameters due to the very complex signal mechanism of the SSFP sequence. The observed signal contrast is therefore rather fat- and T_2^*-weighted than diffusion-weighted. The intermediate diffusion weighting of the applied SSFP sequence, however, helps to shift the different contrasts into a signal range that is easily visually accessible.

Acknowledgements

This work was supported by the Deutsche Forschungsgemeinschaft (DFG), grant no. DI 1413/1-1.

References

1. Charles-Edwards EM, Desouza NM. Diffusion-weighted magnetic resonance imaging and its application to cancer. Cancer Imaging. 2006;6:135-143.
2. Klauss M, Lemke A, Grunberg K, et al. Intravoxel incoherent motion MRI for the differentiation between mass forming chronic pancreatitis and pancreatic carcinoma. Invest Radiol. 2011;46:57-63.
3. Takahara T, Kwee TC, Van Leeuwen MS, et al. Diffusion-weighted magnetic resonance imaging of the liver using tracking only navigator echo: feasibility study. Invest Radiol. 2010;45:57-63.
4. Dale BM, Braithwaite AC, Boll DT, et al. Field strength and diffusion encoding technique affect the apparent diffusion coefficient measurements in diffusion-weighted imaging of the abdomen. Invest Radiol. 2010;45:104-108.
5. Karaarslan E, Arslan A. Diffusion weighted MR imaging in non-infarct lesions of the brain. Eur J Radiol. 2008;65:402-416.

6. Schaefer PW, Copen WA, Lev MH, et al. Diffusion-weighted imaging in acute stroke. Magn Reson Imaging Clin N Am. 2006;14:141-168.
7. Dietrich O, Biffar A, Baur-Melnyk A, et al. Technical aspects of MR diffusion imaging of the body. Eur J Radiol. 2010;76:314-322.
8. Stejskal EO, Tanner JE. Spin diffusion measurements: spin echoes in the presence of a time-dependent field gradient. J Chem Phys. 1965;42:288-292.
9. Gyngell ML. The application of steady-state free precession in rapid 2DFT NMR imaging: FAST and CE-FAST sequences. Magn Reson Imaging. 1988;6:415-419.
10. Bruder H, Fischer H, Graumann R, et al. A new steady-state imaging sequence for simultaneous acquisition of two MR images with clearly different contrasts. Magn Reson Med. 1988;7:35-42.
11. Le Bihan D. Intravoxel incoherent motion imaging using steady-state free precession. Magn Reson Med. 1988;7:346-351.
12. Merboldt KD, Hanicke W, Gyngell ML, et al. Rapid NMR imaging of molecular self-diffusion using a modified CE-FAST sequence. J Magn Reson. 1989;82:115-121.
13. Kaiser R, Barthold.E, Ernst RR. Diffusion and field-gradient effects in NMR Fourier spectroscopy. J Chem Phys. 1974;60:2966-2979.
14. Wu EX, Buxton RB. Effect of diffusion on the steady-state magnetization with pulsed field gradients. J Magn Reson. 1990;90:243-253.
15. Buxton RB. The diffusion sensitivity of fast steady-state free precession imaging. Magn Reson Med. 1993;29:235-243.
16. Freed DE, Scheven UM, Zielinski LJ, et al. Steady-state free precession experiments and exact treatment of diffusion in a uniform gradient. J Chem Phys. 2001;115:4249-4258.
17. Deoni SC, Peters TM, Rutt BK. Quantitative diffusion imaging with steady-state free precession. Magn Reson Med. 2004;51:428-433.
18. Baur A, Stabler A, Bruning R, et al. Diffusion-weighted MR imaging of bone marrow: differentiation of benign versus pathologic compression fractures. Radiology. 1998;207:349-356.
19. Frager D, Elkin C, Swerdlow M, et al. Subacute osteoporotic compression fracture: misleading magnetic resonance appearance. Skeletal Radiol. 1988;17:123-126.
20. Yuh WT, Zachar CK, Barloon TJ, et al. Vertebral compression fractures: distinction between benign and malignant causes with MR imaging. Radiology. 1989;172:215-218.
21. Baker LL, Goodman SB, Perkash I, et al. Benign versus pathologic compression fractures of vertebral bodies: assessment with conventional spin-echo, chemical-shift, and STIR MR imaging. Radiology. 1990;174:495-502.
22. Castillo M, Arbelaez A, Smith JK, et al. Diffusion-weighted MR imaging offers no advantage over routine noncontrast MR imaging in the detection of vertebral metastases. AJNR Am J Neuroradiol. 2000;21:948-953.
23. Baur A, Huber A, Ertl-Wagner B, et al. Diagnostic value of increased diffusion weighting of a steady-state free precession sequence for differentiating acute benign osteoporotic fractures from pathologic vertebral compression fractures. AJNR Am J Neuroradiol. 2001;22:366-372.
24. Spuentrup E, Buecker A, Adam G, et al. Diffusion-weighted MR imaging for differentiation of benign fracture edema and tumor infiltration of the vertebral body. AJR Am J Roentgenol. 2001;176:351-358.
25. Yasumoto M, Nonomura Y, Yoshimura R, et al. MR detection of iliac bone marrow involvement by malignant lymphoma with various MR sequences including diffusion-weighted echo-planar imaging. Skeletal Radiol. 2002;31:263-269.
26. Byun WM, Shin SO, Chang Y, et al. Diffusion-weighted MR imaging of metastatic disease of the spine: assessment of response to therapy. AJNR Am J Neuroradiol. 2002;23:906-912.
27. Baur A, Huber A, Durr HR, et al. [Differentiation of benign osteoporotic and neoplastic vertebral compression fractures with a diffusion-weighted, steady-state free precession sequence]. Rofo. 2002;174:70-75.
28. Abanoz R, Hakyemez B, Parlak M. [Diffusion-weighted imaging of acute vertebral compression: Differential diagnosis of benign versus malignant pathologic fractures]. Tani Girisim Radyol. 2003;9:176-183.
29. Park SW, Lee JH, Ehara S, et al. Single shot fast spin echo diffusion-weighted MR imaging of the spine; Is it useful in differentiating malignant metastatic tumor infiltration from benign fracture edema? Clin Imaging. 2004;28:102-108.
30. Hacklander T, Scharwachter C, Golz R, et al. [Value of diffusion-weighted imaging for diagnosing vertebral metastases due to prostate cancer in comparison to other primary tumors]. Rofo. 2006;178:416-424.
31. Byun WM, Jang HW, Kim SW, et al. Diffusion-weighted magnetic resonance imaging of sacral insufficiency fractures: comparison with metastases of the sacrum. Spine (Phila Pa 1976). 2007;32:E820-824.
32. Karchevsky M, Babb JS, Schweitzer ME. Can diffusion-weighted imaging be used to differentiate benign from pathologic fractures? A meta-analysis. Skeletal Radiol. 2008;37:791-795.
33. Wehrli FW, Ford JC, Attie M, et al. Trabecular structure: preliminary application of MR interferometry. Radiology. 1991;179:615-621.
34. Majumdar S, Thomasson D, Shimakawa A, et al. Quantitation of the susceptibility difference between trabecular bone and bone marrow: experimental studies. Magn Reson Med. 1991;22:111-127.
35. Biffar A, Baur-Melnyk A, Schmidt GP, et al. Multiparameter MRI assessment of normal-appearing and diseased vertebral bone marrow. Eur Radiol. 2010;20:2679-2689.
36. Szumowski J, Coshow WR, Li F, et al. Phase unwrapping in the three-point Dixon method for fat suppression MR imaging. Radiology. 1994;192:555-561.
37. Coombs BD, Szumowski J, Coshow W. Two-point Dixon technique for water-fat signal decomposition with B0 inhomogeneity correction. Magn Reson Med. 1997;38:884-889.
38. Biffar A, Schmidt GP, Baur-Melnyk A, et al. Assessment of benign and malignant vertebral fractures based on the measurement of the fat-fraction. Proc Intl Soc Mag Reson Med. 2010;18:3208.
39. R Development Core Team. R: A language and environment for statistical computing. Vienna: R Foundation for Statistical Computing 2008.
40. Ward R, Caruthers S, Yablon C, et al. Analysis of diffusion changes in posttraumatic bone marrow using navigator-corrected diffusion gradients. AJR Am J Roentgenol. 2000;174:731-734.
41. Lehnert A, Machann J, Helms G, et al. Diffusion characteristics of large molecules assessed by proton MRS on a whole-body MR system. Magn Reson Imaging. 2004;22:39-46.
42. Dietrich O, Biffar A, Reiser MF, et al. Diffusion-weighted imaging of bone marrow. Semin Musculoskelet Radiol. 2009;13:134-144.
43. Schellinger D, Lin CS, Lim J, et al. Bone marrow fat and bone mineral density on proton MR spectroscopy and dual-energy X-ray absorptiometry: their ratio as a new indicator of bone weakening. AJR Am J Roentgenol. 2004;183:1761-1765.
44. Griffith JF, Yeung DK, Antonio GE, et al. Vertebral bone mineral density, marrow perfusion, and fat content in healthy men and men with osteoporosis: dynamic contrast-enhanced MR imaging and MR spectroscopy. Radiology. 2005;236:945-951.
45. Yeung DK, Wong SY, Griffith JF, et al. Bone marrow diffusion in osteoporosis: evaluation with quantitative MR diffusion imaging. J Magn Reson Imaging. 2004;19:222-228.